NEOPLASIA
www.neoplasia.com

Volume 23 Number xxx Month 2021 pp. 1307–1317

Original Research

Amelioration of muscle wasting by gintonin in cancer cachexia

Yoseph Toni Wijaya [a,1]; Tania Setiawan [a,1]; Ita Novita Sari [b]; Seung-Yeol Nah [c]; Hyog Young Kwon [a,b,*]

[a] Department of Integrated Biomedical Science, Soonchunhyang University, Cheonan-si 31151, Republic of Korea
[b] Soonchunhyang Institute of Medi-bio Science (SIMS), Soonchunhyang University, Cheonan-si 31151, Republic of Korea
[c] Ginsentology Research Laboratory and Department of Physiology, College of Veterinary Medicine, Konkuk University, Seoul 05029, Republic of Korea

Abstract

Cancer cachexia is characterized by systemic inflammation, protein degradation, and loss of skeletal muscle. Despite extensive efforts to develop therapeutics, only few effective treatments are available to protect against cancer cachexia. Here, we found that gintonin (GT), a ginseng-derived lysophosphatidic acid receptor (LPAR) ligand, protected C2C12 myotubes from tumor necrosis factor α (TNFα)/interferon γ (IFNγ)- induced muscle wasting condition. The activity of GT was found to be dependent on LPAR/Gαi2, as the LPAR antagonist Ki16425 and Gαi2 siRNA abolished the anti-atrophic effects of GT on myotubes. GT suppressed TNFα-induced oxidative stress by reducing reactive oxygen species and suppressing inflammation-related genes, such as interleukin 6 (IL-6) and NADPH oxidase 2 (NOX-2). In addition, GT exhibited anti-atrophy effects in primary normal human skeletal myoblasts. Further, GT protected against Lewis lung carcinoma cell line (LLC1)-induced cancer cachexia in a mouse model. Specifically, GT rescued the lower levels of grip strength, hanging, and cross-sectional area caused by LLC1. Collectively, our findings suggest that GT may be a good therapeutic candidate for protecting against cancer cachexia.

Neoplasia (2021) 23, 1307–1317

Keywords: Gintonin, Muscle atrophy, Cancer cachexia, Oxidative stress

Introduction

Skeletal muscle mass represents approximately 40–50% of human body weight and serves as both the largest tissue mass and the major protein storage in the body [1]. Most patients with advanced cancer, especially lung cancer, eventually develop a skeletal muscle wasting condition known as cancer-induced cachexia, which is characterized by systemic inflammation, protein degradation, and loss of lean body mass [2]. Cachexia is also observed in many other medical conditions, such as acquired immunodeficiency syndrome (AIDS), chronic obstructive pulmonary disease (COPD), diabetes, and hormonal deficiency [2,3]. In cancer cachexia, the loss of skeletal muscle is the most obvious symptom because it occurs rapidly in cancer patients [4,5]. Up to 60% of cancer patients suffer from cancer cachexia, leading to pronounced weight loss, markedly lower quality of life, and poor prognosis and outcomes [5,6]. Further, cancer cachexia contributes to increase the mortalities of 20 - 30% of cancer patients [7,8].

Cachexia is driven by variable conditions, such as altered energy balance, increased production of pro-cachexia cytokines and factors, and adipose tissue depletion [5]. The major well-known cachexia-inducing factors are myostatin, activin, growth differentiation factor 15 (GDF15), tumor necrosis factor-like weak inducer of apoptosis (TWEAK), and inflammatory cytokines, such as interferon γ (IFNγ), tumor necrosis factor α (TNFα), interleukin 1α and β (IL-1α and IL-1β), and interleukin (IL)-6 [5,9]. These factors lead to catabolic conditions by inducing proteolysis through activation of the ubiquitin-proteasome system (UPS) and autophagy-lysosome system (ALS). During physiological conditions, serine/threonine-protein kinase

* Corresponding author.
E-mail address: hykwon@sch.ac.kr (H.Y. Kwon).
[1] These authors contributed equally to this work.
Received 15 August 2021; received in revised form 11 October 2021; accepted 8 November 2021

https://doi.org/10.1016/j.neo.2021.11.008

(AKT) phosphorylates the FoxO3, leading to cytoplasmic localization. In the cachexia condition, AKT activity is suppressed either by the influence of inflammatory cytokines or the decreased levels of insulin-like growth factor 1 (IGF1). Decreased AKT activity leads to dephosphorylation and subsequent nuclear translocation of FoxO3a proteins, which in turn enable the transcription of Murf-1 and Atrogin-1 [5]. A common converging step that controls inflammatory cytokines involves the nuclear factor kappa B (NF-κB), a ubiquitous transcription factor that mediates cellular responses to a diverse array of stimuli, including lipopolysaccharide, reactive oxygen species (ROS), and several cytokines [10,11]. TNF-α was demonstrated to upregulate inflammatory cytokines via NF-κB, which act as an upstream element of a common pathway that produces catabolic cytokines [9,12]

Ginseng, the root of Panax ginseng Meyer, has been used as a conventional medicinal plant for many centuries in the Orient, particularly in Korea, Japan, and China. The name Panax suggests 'all healing,' which represents the traditional belief that ginseng has characteristics to heal all aspects of the body. Ginseng roots and root extracts have been traditionally used as a medicine in Korea to revitalize the body and mind, increase muscle and physical strength, prevent aging, and increase vigor [13,14]. Panax ginseng (Korean ginseng) was demonstrated to induce muscle strength of normal mice after 7 weeks of treatment [15] and reduce muscle damage and inflammatory response in mice caused by eccentric muscle contraction [16]. Several ginsenosides, such as ginsenoside Rg1, have also been demonstrated to have protective effects on muscle by up-regulating promyogenic kinases on C2C12 myoblasts cells [17]. Thus, we hypothesized that ginseng might have a potential beneficial effect on muscle atrophy. Here, we screened ginseng-derived components and identified that gintonin (GT), a ginseng-derived lysophosphatidic acid receptor (LPAR) ligand, enhanced the myotube diameter and fusion of both mouse C2C12 and human skeletal myoblast (HSkM) cells. Using a murine model, we also showed that GT protected against Lewis lung carcinoma cell line (LLC1) -induced cancer cachexia *in vivo*.

Results

Ginseng-derived components induce hypertrophy and fusion of C2C12 myotubes

We hypothesized that ginseng-derived components may have potential effects on muscle atrophy. To prove this hypothesis, we screened various ginseng-derived components (arginine-fructose-glucose (AFG), GT, non-saponin extracts, and total saponin extracts at 100 ng/ml; ginsenoside Rb1, Rb2, Rc, Rd, Re, Rf, Rg1, Rg2, Rg3R, and Rg3 isomer such as Rg3R, and Rg3S at 100 nM) to determine their potential effects on C2C12 myotubes. Myoblast C2C12 cells were differentiated into myotubes and then treated with ginseng-derived components for 2 days. The cell hypertrophy and fusion index were determined by measuring cell diameter and counting the number of nuclei per cell, respectively. To quantify the myotube diameter, MHC-positive myotubes with more than 10 nuclei were counted in 10 different places, and the diameter mean was calculated. To quantify cell fusion induced by ginseng components, we calculated the fusion index by counting the number of nuclei per MHC-positive myocytes (mononucleate, two to five nuclei, and six or more nuclei per myotube). Several ginsenosides, such as ginsenoside Rd, Rb1, Rg2, Rg3R, and Rg3S, induced cell hypertrophy and fusion (Supplementary Fig. 1). This finding is consistent with that of previous reports, where ginsenoside Rb1 and Rg3 were shown to induce muscle hypertrophy and myoblast differentiation [18,19]. Interestingly, we found that GT (100 ng/ml) markedly induced the highest levels of hypertrophy and fusion of C2C12 myotubes among the ginseng components tested (Supplementary Fig. 1).

GT induced hypertrophy and fusion of C2C12 myotubes

As GT strongly exhibited hypertrophic effects on myotubes compared to other ginsenosides, we proceeded to determine whether GT has protective effects on muscle wasting. First, we tested the effect of GT on C2C12 cell viability. GT treatment did not display apparent cytotoxicity against C2C12 myotubes (Supplementary Fig. 1). To determine the dose-dependent hypertrophic effects of GT on myotubes, C2C12 myotubes were treated with 10 ng/mL to 10,000 ng/mL GT and stained with a myosin heavy chain (MHC), a marker of myogenic differentiation. GT treatment increased myotube diameter approximately by 2.5-fold compared to the control (Fig. 1A, B). GT also significantly increased the frequency of myotubes containing multiple nuclei (2 to 5 nuclei and six or more nuclei) compared to control (Fig. 1A, C). Moreover, the frequency of mononucleate myocytes was significantly lower with GT treatment (Fig. 1A, C), suggesting that GT promoted the formation of bigger myotubes by inducing muscle cell fusion.

GT protects C2C12 myotubes from TNFα/IFNγ - induced muscle cell atrophy

As GT increased the muscle cell size and fusion index, we questioned whether GT could protect muscle cells from cancer cachexia condition. To mimic cancer cachexia *in vitro,* differentiated C2C12 cells were treated with TNFα/IFNγ (TI) together with GT and the effects of GT on cellular atrophy were determined. The decreased myotube diameters caused by TI were significantly increased by GT treatment in a dose-dependent manner (Fig. 1D, E). Moreover, the frequency of myotubes with multiple nuclei was significantly increased with GT+TI treatment compared to TI alone (Fig. 1D, F). To determine a potential therapeutic effect of GT, C2C12 cells were pretreated with TI and then GT was added. Consistent with co-treatment of GT+TI, GT exerted protective effects on pretreated TI-induced cellular atrophy (Fig. G–I). To test whether these effects were associated with proteolysis-related proteins, such as Atrogin-1 and MuRF-1, we determined the expression of these proteins. As expected, Atrogin-1 and MuRF-1 were induced by TI, which was significantly reduced by GT (Fig. 1J, K). Altogether, these results indicate that GT protected C2C12 myotubes from TI-induced muscle cell atrophy.

GT protects against cellular atrophy through the lysophosphatidic acid receptor (LPAR)

Previously, it was shown that GT activates lysophosphatidic acid receptors (LPAR) and suppresses heat stress-induced inflammation through LPAR [20,21]. Thus, to gain insights into the mechanisms of GT, we tested whether the effects of GT on muscle cells are associated with LPAR. First, we determined whether LPAR (LPAR1, LPAR2, and LPAR3) expression is affected in C2C12 cells by GT using RT-qPCR. The expression of both LPAR1 and LPAR3, but not LPAR2, was significantly induced with GT treatment (Fig. 2A). Further, we determined whether LPAR is functionally related to GT using the LPAR antagonist Ki16425. Differentiated C2C12 myotubes were pre-treated with Ki16425 for 30 min, followed by GT treatment. Thereafter, the diameter and fusion index of myotubes were determined. The diameter and fusion index induced by GT were significantly decreased with the dual treatment of GT and Ki16425 (Fig. 2B–D), suggesting that GT induces muscle cell hypertrophy via LPAR. As a proof-of-concept, we tested the effects of the LPAR agonist, LPA, on myotubes, and found that LPA at 20 μM also induced the hypertrophy of myotubes (Fig. 2B–D). Gai2, a downstream signaling protein of LPA/LPAR, was demonstrated to promote muscle hypertrophy by stimulating PI3K-AKT to induce cell growth and inhibiting protein degradation through the reduction of E3 ubiquitin ligase atrogin-1 [22–25]. Using Gαi2 siRNA, we tested whether the hypertrophic effects of GT are associated with Gαi2. As shown,

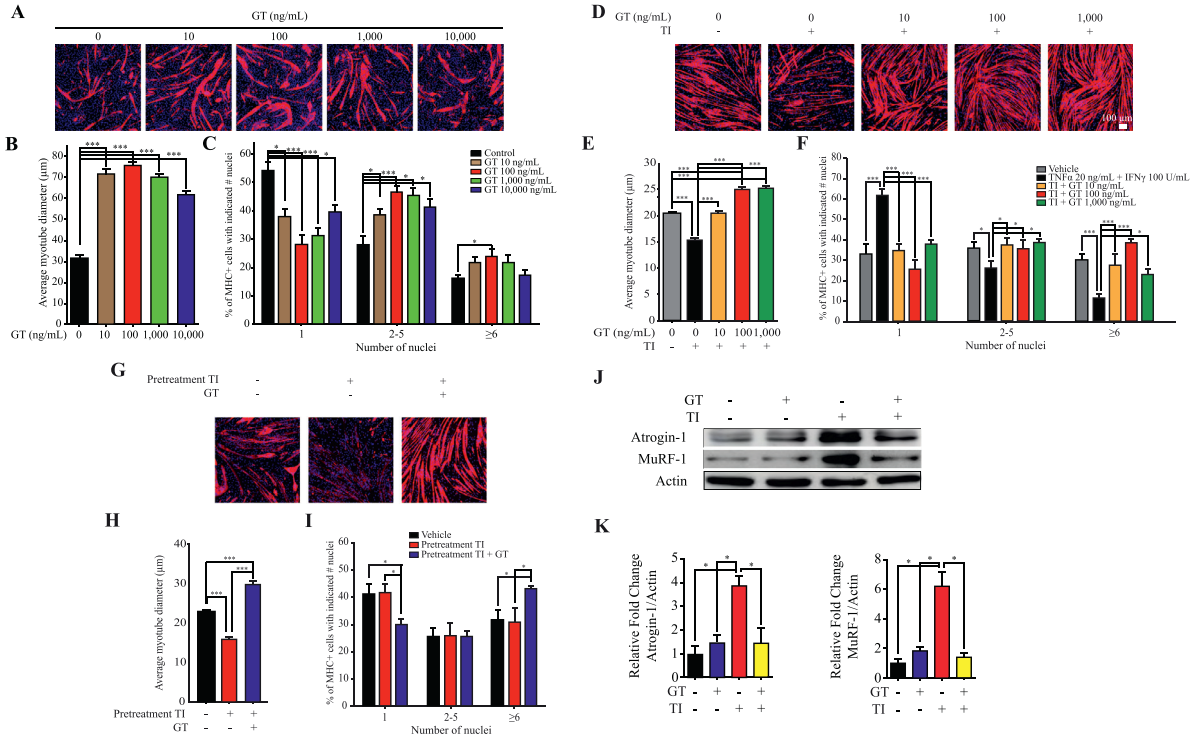

Fig. 1. GT protects C2C12 myotubes from TNFα/IFNγ-induced muscle cell atrophy.
(A-C) C2C12 myotubes were treated with GT for 48 h at the indicated concentration and stained with anti-MHC Ab. (A) Representative images were shown. (B) Average myotube diameter was measured by ImageJ software. (C) The number of nuclei per myotube was quantified. The data were shown as mean ± SEM of more than 100 myotubes from 10 randomly chosen fields (*$P \leq 0.05$; ***$P \leq 0.0001$). (D-F) C2C12 myotubes were treated with GT at the indicated concentrations together with TNFα (20 ng/mL) and IFNγ (100U/mL) for 24 h, and then stained with anti-MHC Ab. (D) Representative images were shown. (E) Average myotube diameter was measured by ImageJ software. (F) The number of nuclei per myotube was quantified. The data were shown as mean ± SEM of more than 100 myotubes from 10 randomly chosen fields (*$P \leq 0.05$; ***$P \leq 0.0001$). (G-I) C2C12 myotubes were pre-treated with TNFα (20 ng/mL) and IFNγ (100U/mL) for 24 h, and then treated with GT (100 ng/mL) for 24 h. Cells were stained with anti-MHC Ab. (G) Representative images were shown. (H) Average myotube diameter was measured by ImageJ software. (I) The number of nuclei per myotube was quantified. The data were shown as mean ± SEM of more than 100 myotubes from 10 randomly chosen fields (*$P \leq 0.05$; ***$P \leq 0.0001$). (J-K) C2C12 myotubes were treated with GT (100 ng/mL) together with TNFα (20 ng/mL) and IFNγ (100U/mL). Cells were isolated, and the protein levels of Atrogin-1 and MuRF-1 were evaluated by western blot. (J) Representative images were shown. (K) Images were measured by ImageJ software. The data were shown as mean ± SEM (n=3; *$P \leq 0.05$).

GT induced the hypertrophy of C2C12 myotubes, which was abolished with two independent Gαi2 siRNA (Fig. 2E–I). These results suggest that GT protects against cellular atrophy through the LPAR/Gαi2 pathway.

GT protects C2C12 cells from oxidative stress

As oxidative stress is a common mechanism of cancer cachexia [26] and GT was demonstrated to reduce inflammatory response [21], we hypothesized that GT could reduce oxidative stress or inflammation, protecting C2C12 myoblast from oxidative damage caused by TNFα. To prove this hypothesis, we determined total ROS levels in C2C12 cells using 2',7'–dichlorofluorescein diacetate (DCFDA) in the absence or presence of TNFα. As expected, TNFα induced higher levels of ROS than the vehicle (Fig. 3A, B). Interestingly, the accumulated ROS levels caused by TNFα were significantly reduced by GT or the well-known ROS scavenger, N-acetylcysteine (NAC) (Fig. 3A, B). The reduction of ROS levels by GT was also observed in C2C12 myotubes (Fig. 3C, D). Using MitoSox™ Red mitochondrial superoxide indicator, we also determined mitochondrial ROS levels. The levels of mitochondrial ROS were consistently reduced by GT treatment (Fig. 3E, F). As a higher level of ROS is known to reduce mitochondrial membrane potential (ΔΨm), we tested whether GT could rescue mitochondrial membrane potential using a MitoProbe $DiIC_1(5)$ assay kit. TNFα was found to induce the ΔΨm collapse in C2C12 myoblast; however, this was rescued by the addition of GT (Fig 3G, H).

Thus, to identify the mechanisms whereby GT reduces ROS levels, we employed two independent methods: a radical scavenging assay and inflammation-related gene regulation by GT. First, we determined the radical scavenging activity of GT using a hydroxyl radical scavenging assay. The hydroxyl radicals generated from H_2O_2 was dose-dependently reduced by the addition of GT. Interestingly, 1 ng/ml GT displayed a markedly better scavenging effect than the well-known scavenger, ascorbic acid (125 ng/ml) in our system (Fig 3I). Second, the inflammation-related genes, such as NOX2 and IL-6, induced by TNFα are known to be implicated in ROS production [26]. TNFα induced the expression of IL-6 and NOX-2, which was significantly reduced by GT (Fig 3J, K). These results suggest that GT protects against cellular atrophy by exhibiting ROS scavenging activity and reducing inflammation-related genes.

GT protects against atrophy of primary normal human skeletal myoblasts (HSkM)

As GT protected against muscle cell atrophy in a mouse system *in vitro*, we wondered whether the protection by GT is also evident in human cells. Thus, by using HSkM, we analyzed the effect of GT on human muscle cell

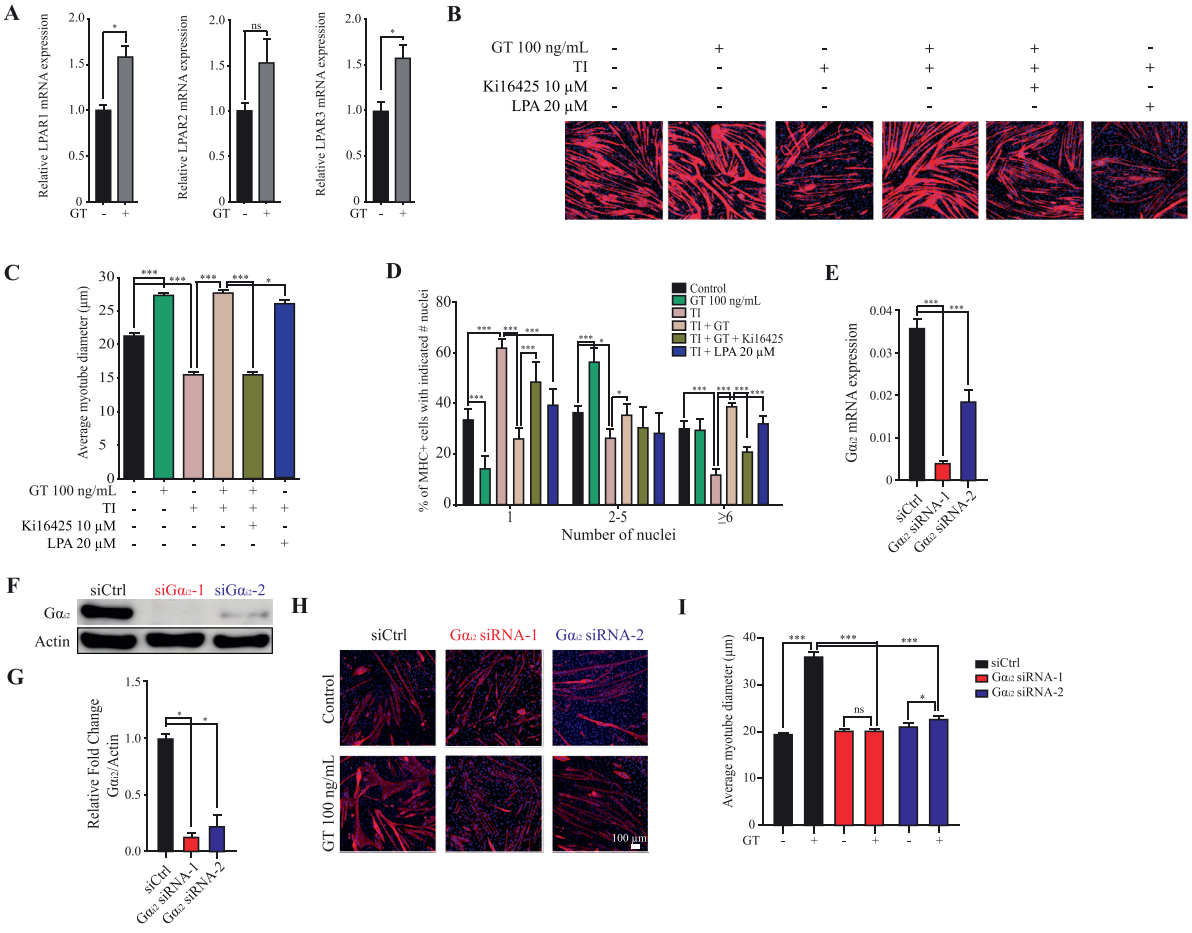

Fig. 2. GT protects against cellular atrophy through the lysophosphatidic acid receptor (LPAR) and Gαi2 activation.
(A) C2C12 myotubes were treated with GT (100 ng/mL) for 24 h and then the expression of LPARs were quantified by RT-PCR. The data were shown as mean ± SEM of three independent experiments (*$P \leq 0.05$; ns, not significant). (B–D) C2C12 myotubes were treated with GT (100 ng/mL), TNFα (20 ng/mL) and IFNγ (100U/mL), or Ki16425 (10 μM) for 24 h and then stained with anti-MHC Ab. (B) Representative images were shown. (C) Average myotube diameters and (D) the number of nuclei per myotube of more than 100 myotubes from 10 randomly chosen fields for each condition were measured by ImageJ software. The data were shown as mean ± SEM (*$P \leq 0.05$; ***$P \leq 0.0001$). (E-F) C2C12 cells were transfected with control (non-targeting) (siCtrl) or Gαi2 siRNA. (E) mRNA level of *Gαi2* was evaluated by RT-PCR and (F, G) protein level of *Gαi2* was evaluated by western blot. The data were shown as mean ± SEM of 2 independent experiments ((*$P \leq 0.05$; ***$P \leq 0.0001$). (H, I) The transfected cells were differentiated to myotubes for 4 days and treated with GT (100 ng/mL) for 48 h. (H) Representative images were shown. (I) Average myotube diameters of more than 100 myotubes from 10 randomly chosen fields of each condition were measured by ImageJ software. The data were shown as mean ± SEM (*$P \leq 0.05$;***$P \leq 0.001$; ns, not significant).

atrophy. HSkM cells were differentiated in low glucose DMEM with 2% horse serum for 7 days, treated with GT for 3 days in the presence or absence of TNFα. Thereafter, the diameter and fusion index of myotubes were determined (Fig. 4A, B). GT-treated HSkM myotubes exhibited significantly larger diameters than the control myotubes (Fig. 4A, B). In addition, the frequency of cells containing more than 5 nuclei was significantly higher in the GT-treated group compared to the control group (Fig. 4C). Consistently, in a TNFα -induced atrophy model, we found that GT increased both the cell diameter and frequency of cells containing more than 5 nuclei (Fig. 4A-C). Further, we also checked the levels of Atrogin-1 and MuRF-1 after TNFα treatment in the absence or presence of GT. Consistent with the results obtained from C2C12 cells, both Atrogin-1 and MuRF1 were highly induced with TNFα in HSkM cells, which was significantly reduced with GT treatment (Fig. 4D, E). These results suggest that GT protects against atrophy of both mouse and human muscle cells and could thus serve as a promising candidate for cancer cachexia.

GT-enriched fraction (GEF) protected against Lewis lung carcinoma (LLC1)-induced cancer cachexia in vivo

To further verify the effect of GT on cancer cachexia *in vivo*, a lung cancer-induced cachexia murine model was employed. To date, it is known that cachexia is the most common problem associated with advanced lung cancer [27,28]. Among the available cancer cachexia models, the Lewis lung carcinoma (LLC1) and colon-26 adenocarcinoma (C26) models are the most commonly used [29–31]. Here, we used the LLC1-induced cancer cachexia model to further elucidate the GT effects in the cachexia inhibition *in vivo*.

For the *in vivo* study, we used GEF, which was mass-produced from ginseng using ethanol and water as shown before [32]. To evaluate the effect of GEF on muscle wasting, LLC1 cells were subcutaneously injected into the flanks of C57BL6 mice. Thereafter, GEF was orally administered daily for 15 days starting at 6 days post tumor implantation. The grip-strength was determined every two days during the treatment (Fig. 5A). The LLC1-

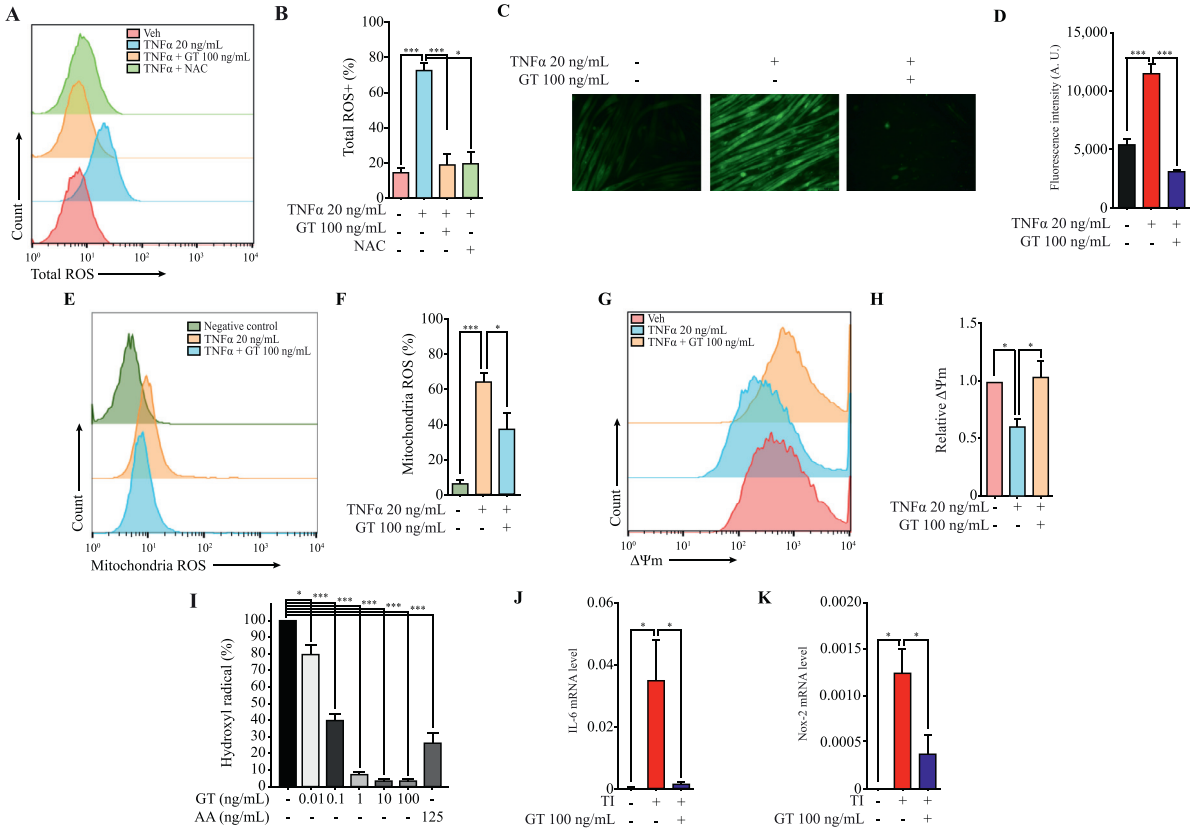

Fig. 3. GT protects C2C12 myoblast from oxidative stress through the reduction of ROS and inflammation genes.
(A, B) C2C12 myoblast was incubated for 4 h with TNFα (20 ng/mL), GT (100 ng/mL), or N-acetyl cysteine (NAC) as indicated, and then ROS levels were measured by flow cytometry. NAC was used as a negative control. (A) Representative FACS profiles were shown and (B) the data were presented as mean ± SEM of four independent experiments ($^{*}P \leq 0.05$; $^{***}P \leq 0.0001$). (C, D) C2C12 myotube was incubated with TNFα (20 ng/mL) and GT (100 ng/mL) for 4 h as indicated, and then ROS levels were measured by fluorescence microscope. (C) Representative fluorescence images were shown and (D) fluorescence intensity were quantified using the ImageJ software. The data were presented as mean ± SEM of at least 10 randomly chosen fields of each condition ($^{***}P \leq 0.0001$). (E, F) C2C12 myoblast was incubated for 24 h with TNFα (20 ng/mL) or GT (100ng/mL) as indicated, and mitochondria ROS were measured by flow cytometry. (E) Representative FACS profiles were shown and (F) the data were presented as mean ± SEM of four independent experiments ($^{*}P \leq 0.05$; $^{***}P \leq 0.0001$). (G, H) C2C12 myoblast was incubated for 24 h with TNFα (20 ng/mL) or GT (100ng/mL) as indicated, and mitochondrial membrane potential ($\Delta\Psi$m) were measured by flow cytometry. (G) Representative FACS profiles were shown and (H) the data were presented as mean ± SEM of five independent experiments ($^{*}P \leq 0.05$). (I) The effect of GT on scavenging of hydroxyl radical was analyzed using iron (II)-dependent TBA reactive substance. Ascorbic acid (AA) was used as a positive control. Data were shown as mean ± SEM of three independent experiments ($^{*}P \leq 0.05$; $^{***}P \leq 0.0001$). (J, K) C2C12 myotubes were treated for 24 h with TI (TNFα at 20 ng/mL and IFNγ at 100U/mL) or GT (100 ng/mL) as indicated, and then the levels of IL-6 (J) and Nox-2 (K) were quantified by RT-PCR. The data were shown as mean ± SEM of three to four independent experiments (*, $P \leq 0.05$).

induced cachexia model was well established, as characterized by an obvious decrease in tumor-free body weight and significant loss of muscle weights compared to that in wild-type control mice (Fig. 5B–E). GEF did not exert any obvious anti-tumor effect, as demonstrated by the similar tumor size between GEF-treated and PBS-treated mice (Fig. 5B). Excitingly, GEF distinctly improved several features of cancer cachexia, including tumor-free body weight, muscle weights, grip strength, and hanging time (Fig. 5C–H). PBS-treated mice (LLC1+PBS) exhibited 9.51% loss of tumor-free body weight compared with the healthy control group, whereas that of GEF-treated mice (LLC+ GEF) was significantly rescued (Fig. 5C). Similarly, the weights of tested muscles, including Soleus (SOL), extensor digitorium longus (EDL), gastrocnemius (GA), and tibialis anterior (TA), were decreased in PBS-treated mice compared to healthy control mice, but were rescued by GEF treatment (Fig. 5D, E). The organ weights tested, such as heart, lungs, and spleen, were not affected by GEF treatment (Fig. 5F). The decreased grip strength was partially rescued by GEF treatment compared to that in healthy control mice during the treatment (day 9 to day 21) (Fig. 5G). Consistently, the lower levels of the hanging test caused by LLC1 was rescued by GEF treatment, which was comparable to that of healthy mice (Fig. 5H). To understand the protective effect of GEF on muscle atrophy at the molecular level, hematoxylin, and eosin (H&E) staining was conducted. The average cross-section area (CSA) with GEF treatment was 1.8-fold higher than that with PBS treatment (Fig. 5 I, J). The PBS-treated group had smaller sizes of CSA distribution, whereas the GEF-treated group exhibited larger sizes of CSA, which were comparable to the sizes observed in healthy mice (Fig. 5I, K). To further investigate the possible anti-cachexia mechanism of GEF, the levels of several muscles atrophy-related signaling pathways, such as myostatin, MuRF-1 and Atrogin-1, in GA muscle were determined by western blot. The levels of myostatin, MuRF-1 and Atrogin-1 was significantly increased in PBS-treated mice compared to that in the healthy mice and were partially rescued by GEF treatment (Fig. 5L, M). These results suggest that GEF could protect against LLC1-induced muscle atrophy *in vivo*.

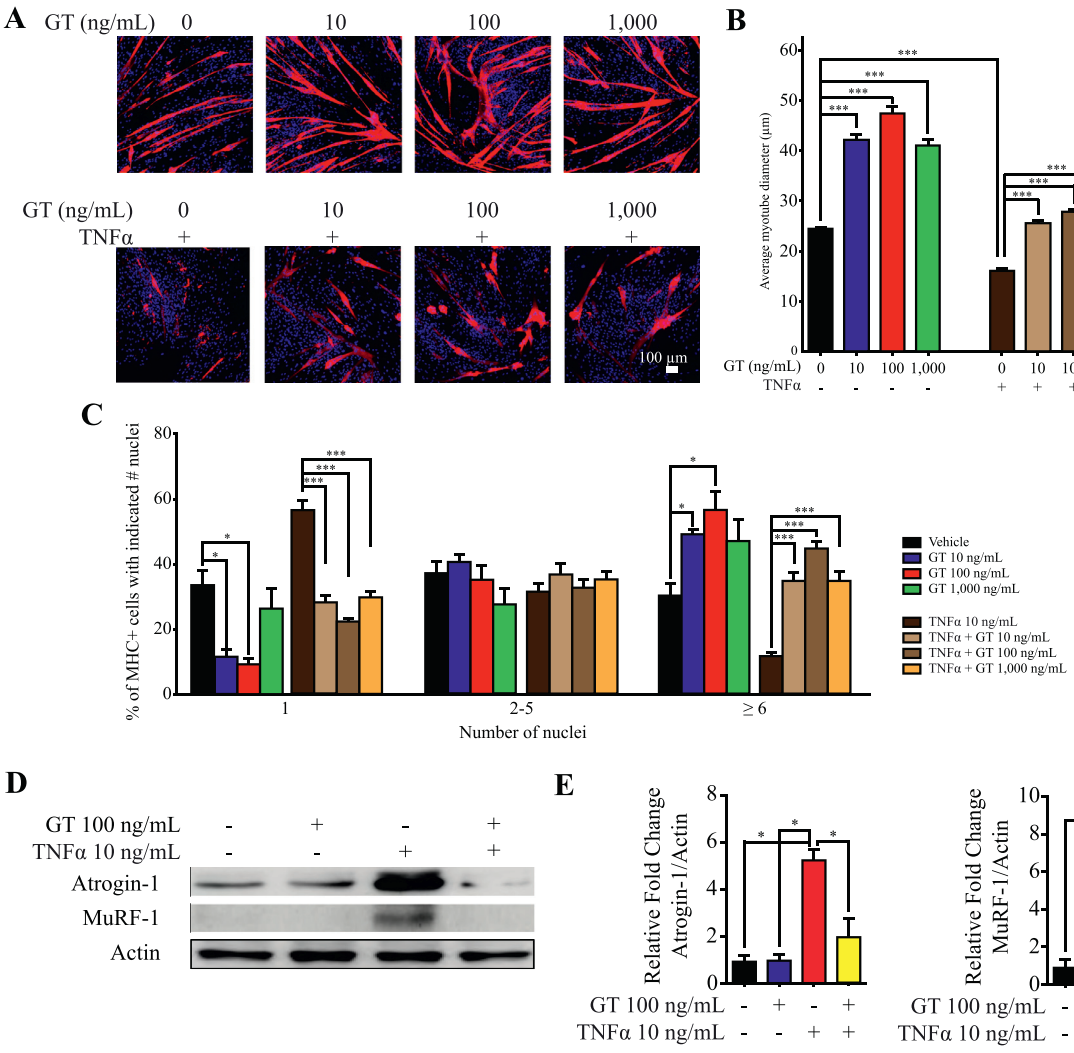

Fig. 4. GT protects against the atrophy of primary normal Human Skeletal Myoblasts (HSkM).
(A–C) HSkM myoblast were differentiated to myotube for 7 days in differentiation media. Differentiated cells were treated with different concentrations of GT in the presence or absence of TNFα (10 ng/mL) for 3 days and then stained with anti-MHC Ab. (A) Representative images of myotube cultures were captured with a phase-contrast microscope (100x magnification). (B) Average myotube diameters and (C) the number of nuclei per myotube were quantified from more than 100 myotubes in 10 randomly chosen fields of each condition using ImageJ software. The data were shown as mean ± SEM ($^{*}P \leq 0.05$; $^{***}P \leq 0.0001$). (D, E) HSkM myotubes were treated with GT (100 ng/mL) together with TNFα (10 ng/mL) for 8 h. Cells then were isolated, and the protein levels of Atrogin-1 and MuRF-1 were evaluated by western blot. (D) Representative images were shown. (E) Images were measured by ImageJ software. The data were shown as mean ± SEM (n=3; $^{*}P \leq 0.05$).

Discussion

Muscle atrophy is observed in various conditions, such as aging, cancer, diabetes, and renal failure, as well as after long periods of inactivity [33]. Cancer cachexia is found in up to 60% of cancer patients and is associated with a poor prognosis [5,6]. Despite extensive efforts to develop therapeutics, only few effective treatments are available to protect against muscle atrophy. In this study, we found that GT, a ginseng-derived component, has skeletal muscle anti-atrophic effects *in vitro* and *in vivo*. GT protected both mouse C2C12 and human HSkM myotubes from TNFα/IFNγ- induced muscle atrophy *in vitro*. In addition, in a cancer cachexia mouse model, GT preserved the tumor-free body weight and grip strength, and improved the muscle masses, including those of GA, SOL, TA, and EDL. However, GT did not show obvious anti-tumor effects at the dose used, suggesting that the anti-cachexia effects of GT may be related to skeletal muscle anti-atrophy, but not to smaller tumor size.

GT is a glycolipoprotein extracted from ginseng that contains lysophosphatidic acid (LPA) [34]. Thus, it is also known as a novel high-affinity ligand for mammalian LPAR [20]. LPARs are well known to be highly expressed in many types of cells and are responsible for proliferation, survival, cytoskeletal changes, and calcium influx [35]. LPAR is a G protein-coupled receptor (GPCR) that couples to heterotrimeric G proteins (Gαi2, Gq, G12/13 alpha subunits) and can evoke multiple cellular responses upon LPA stimulation [35]. The biological activity of LPA is largely mediated via the activation of the six receptors, LPAR1 to LPAR6 [35]. Of these receptors, we found that GT treatment induced the expression of both LPAR1 and LPAR3. The activity of GT was dependent on the LPAR/Gαi2 signaling pathways, as evidenced by that both the LPAR antagonist Ki16425 and siGαi2 abolished the effects of GT on C2C12 myotubes. Consistently, the anti-atrophic effect of Gαi2 was revealed in a previous report, indicating that Gαi2 inhibits TNFα-induced atrophy effects by acting as a counterbalance to MuRF-1 and Atrogin 1-mediated atrophy [25,36]. Thus, we propose that

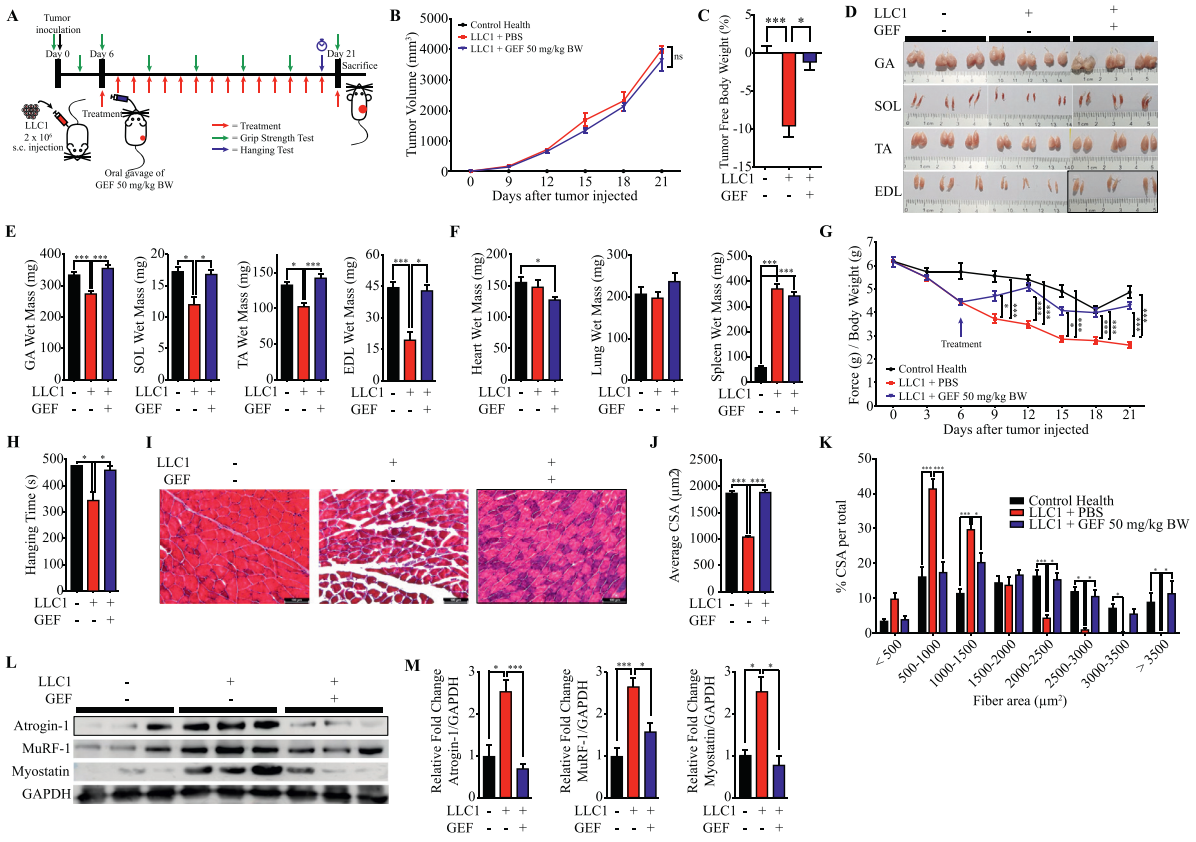

Fig. 5. GEF protected against Lewis lung carcinoma (LLC1)-induced cancer cachexia *in vivo*
(A) Experiment design of LLC1-induced cancer cachexia. Mice were injected subcutaneously with LLC1 cells. Then, after 6 days of injection, mice were orally administrated with GEF (50 mg/kg body weight/day) or PBS daily for 15 days. Control (n=8), LLC1 + PBS (n=6), and LLC1 + GEF 50 mg/kg (n=6). (B) Tumor volume and (C) body weight were determined. (D-F) skeletal muscles, including GA, SOL, TA, and EDL, and organs (heart, lungs, and spleen) were dissected at 21 days. (D) Representative images of skeletal muscles were shown, and weights of skeletal muscles (D) and organs (F) were determined. The data were shown as mean ± SEM ($^{*}P \leq 0.05$; $^{***}P \leq 0.0001$). (G) Grip strength was evaluated every 3 days and (H) hanging test was conducted at day 20. The data were shown as mean ± SEM ($^{*}P \leq 0.05$; $^{***}P \leq 0.0001$). (I–K) GA muscles were stained with HE staining, and (I) representative images were shown. (J) Average of cross-sectional area (CSA) GA muscle fiber was quantified by ImageJ and (K) plotted depending on the frequency as indicated. The data were shown as mean ± SEM ($^{*}P \leq 0.05$; $^{***}P \leq 0.0001$). (L–M) GA tissue lysates were isolated, and the protein level of muscle atrophy-related genes were evaluated by western blot. (L) Representative images were shown. (M) Images were measured by ImageJ software. The data were shown as mean ± SEM (n=6; $^{*}P \leq 0.05$).

GT prevents muscle atrophy via activation of the LPAR/ Gαi2 signaling pathway.

The other mechanism, we propose, by which GT protects against cancer cachexia is via ROS reduction. Previously, it was shown that GT reduced the ROS levels through activation of the LPAR1 receptor signaling pathway in HT22 and that ROS levels were reduced through LPA3 receptor activation in HEK293 cells [37,38]. We also discovered that GT treatment decreased ROS levels through the reduction of inflammation-related genes, such as NOX2 and IL6, and ROS scavenging activity of GT. Thus, it seems that LPAR activation plays important roles in ROS reduction. Although it has been revealed that GT has a ROS scavenging activity via biochemical analysis *in vitro*, it is not clear yet whether GT enters cells and scavenges ROS directly inside cells, independent of LPAR activation. However, it was observed that LPA3/LPAR were internalized via lysosomal pathway in progerin HEK293 cells [38], indicating that the possibility of GT internalization should not be completely excluded, and remain to be addressed and further studied.

GT was demonstrated to have potential neuroprotective effects against several models of neurodegenerative diseases, such as Alzheimer disease (AD) and multiple sclerosis [39–42]. GT was also revealed to suppress oxidative stress and inflammatory response caused by heat stress in C2C12 cells [21]. In addition, in an animal model of experimental autoimmune encephalomyelitis (EAE), GT was shown to alleviate EAE due to its anti-inflammatory and antioxidant activities [42]. These phenotypes were mechanistically achieved by the inhibition of the ERK, p38 mitogen-activated protein kinases (MAPKs), and NF-κB pathways, and the stabilization of nuclear factor erythroid 2-related factor 2 (Nrf2) via increased expression of LPAR1–3 [42]. Here, we also found that GT exhibited anti-oxidant effects by directly scavenging ROS and reducing inflammation-related genes, such as IL6 and NOX2. Thus, it seems that GT can reduce the inflammatory response in many types of tissues, including muscle and neuronal system. Previously, we showed that GEF administration was safe and tolerated by cognitively impaired elderly subjects, and exhibited potential beneficial effects on cognition in the participants from the small scale of clinical trial [43]. Thus, we propose that GEF is a good therapeutic candidate to protect against or alleviate cancer cachexia-associated signaling and inflammatory response, and could be tested clinically to improve muscle wasting.

In summary, we found that the novel ginseng component, GT, induced hypertrophy and fusion in both mouse and human myotubes. GT also protected against or alleviated LLC1-induced muscle wasting in a mouse

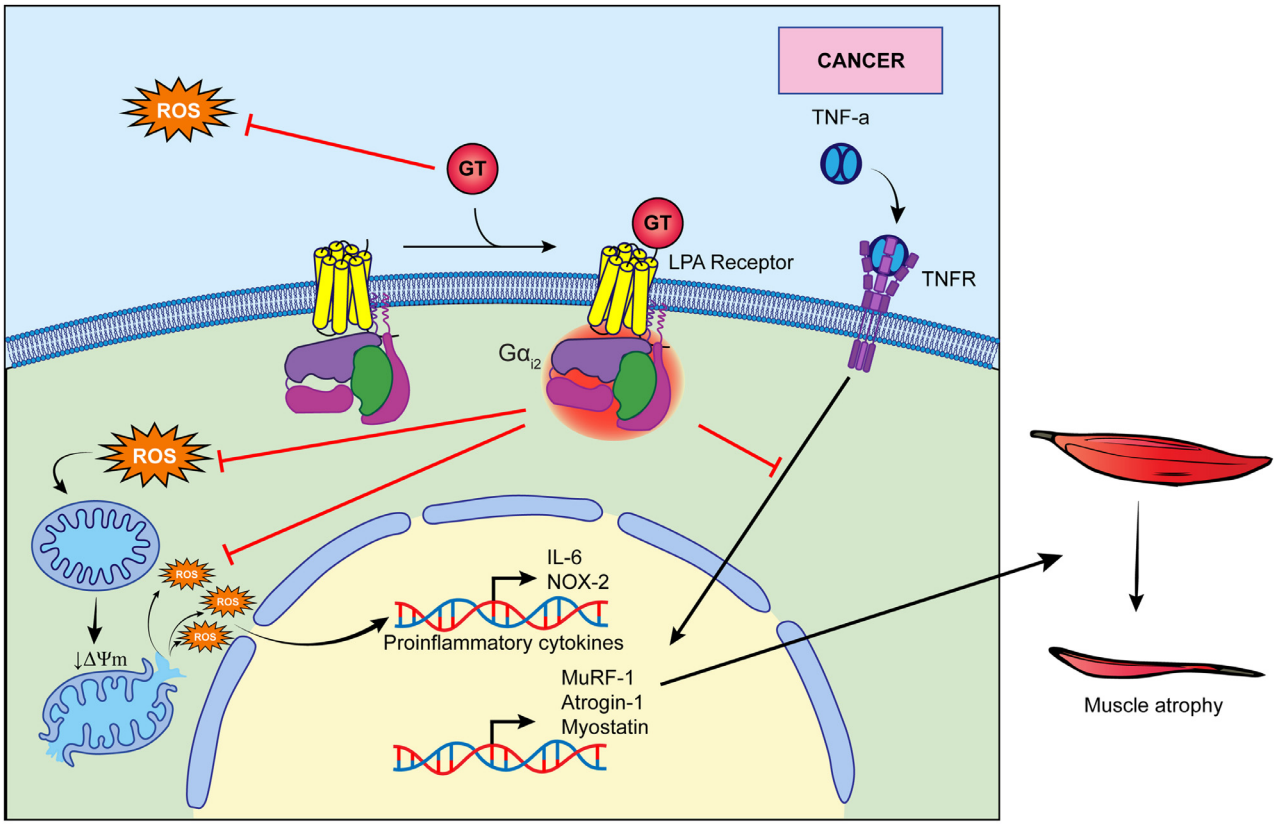

Fig. 6. A model of the molecular pathway of GT against cancer cachexia.
GT binds to the LPA receptor, leading to the activation of Gαi2. Gαi2 activation inhibits TNFα-induced atrophy by repression of muscle atrophy and inflammation-related genes. In addition, GT reduces oxidative stress, inhibiting the loss of mitochondrial membrane potential.

model through LPAR and Gαi2 (Fig. 6). Thus, we propose that GT could be a promising candidate to treat skeletal muscle atrophy under both physiological and pathological conditions.

Materials and methods

Preparation of GT and GEF

GT and GEF was prepared as described before [44–46]. Briefly, to prepare GT from ginseng root, eight kilograms of 4-year-old ginseng roots were ground into small pieces (> 3 mm) and refluxed with 80% methanol (MeOH) three times for 8 h at 80°C each. The MeOH extracts (1.3 kg) concentrated in vacuo were partitioned between n-butanol (n-BuOH) and water. n-BuOH fraction (fr., 300 g) of Panax ginseng dissolved in phosphate buffer saline (PBS, pH 7.2) was loaded onto a column packed with DEAE sepharose CL-6B (GE Healthcare) and equilibrated with PBS (pH 7.2). The unbound materials were eluted with the same buffer and the bound materials were eluted with a linear gradient of 0 to 1 M NaCl in PBS (pH 7.2). The eluted fraction was further dialyzed at 4°C for 8 h with 1000-fold excess distilled water (DW) using Spectra/Por dialysis membrane (molecular weight cut off 6000–8000; Spectrum Laboratories Inc., Rancho Dominguez, CA, USA) to remove small molecular components such as ginsenosides and other components with a yield of 0.2% (Pyo, 2011 #134). To prepare GEF from ginseng root, one kilogram of 4-year-old ginseng was ground into small pieces (> 3 mm) and refluxed with 70% fermentation ethanol eight times for 8 h at 80°C each. The ethanol extracts (150 g) were concentrated as previously described (Hwang, 2012 #10; Choi, 2015 #17).

Cell culture

The mouse myoblast cell line, C2C12, was obtained from the American Type Culture Collection (Manassas, VA, USA) and cultured in a growth medium (GM, Dulbecco's modified Eagle's medium [DMEM, Corning Life Sciences, Oneonta NY, USA], supplemented with 10% fetal bovine serum [FBS, Corning Life Sciences] and 1% penicillin-streptomycin [Corning Life Sciences] under 5% CO_2 at 37°C. For differentiation, 1×10^5 cells were seeded in each well of 24 well-plates and cultured until confluency, unless stated otherwise. Confluent C2C12 cells were cultured in a differentiation medium (DM, DMEM containing 2% heat-inactivated horse serum [Sigma] and 1% penicillin-streptomycin) for up to 4 days for myogenic differentiation. The differentiation media were replaced every 2 days with fresh differentiation medium. The Human skeletal myoblast (HSkM) cells were obtained from Thermo Fisher Scientific. For differentiation, 1×10^5 cells were seeded in each well of 24 well-plates and cultured until confluency. Cells were differentiated in a differentiation medium (low glucose DMEM [Gibco] containing 2% heat-inactivated horse serum [Sigma] and 1% penicillin-streptomycin) for up to 7 days, treated with GT for 3 days, and then the diameter and fusion index of myotubes were determined. All cytokines were purchased from Peprotech, USA.

Western blot analysis

Tissue lysates were harvested using a homogenizer and lysis with a common cell lysis buffer and centrifuged at 13,000 rpm for 20 min at 4°C. The protein concentration of the supernatant was determined by Bio-Rad Protein Assay (Bio-Rad Laboratories, Inc., USA). An equal amount of each

Table 1

Sequences of RT-qPCR primers used in this study.

	Sense (5′-3′)	Antisense (5′-3′)
LPAR1	AGCCATGAACGAACAACAGTG	CATGATGAACACGCAAACAGTG
LPAR2	TGCTACTACAACGAGACCATCG	ATGGCTGCAATAACCAGCAGA
LPAR3	CAAGCGCATGGACTTTTTCTAC	GAAATCCGCAGCAGCTAAGTT
Gαi2	CAACTCCTCCAGCCTAGACC	TCTCTCACGCTTCTTGTGCT
GAPDH	AGAAGACTGTGGATGGCCCCTC	GATGACCTTGCCCACAGCCTT

protein extract (30 μg) was resolved using 10% polyacrylamide gel and electro-transferred onto 0.45 μm hybridization nitrocellulose filter (HATF) membrane (Millipore, USA) using Trans-blot turbo (Bio-Rad Laboratories, Inc., USA). The following antibodies were used anti-atrogin-1 (sc-166806, Santa Cruz Biotechnology, Texas, USA), anti-MuRF-1 (ab172479, Abcam, MA, USA), anti-GDF8/myostatin (sc-398333, Santa Cruz Biotechnology, Texas, USA), anti-Gai-2 (sc-13534, Santa Cruz Biotechnology, Texas, USA), anti-Actin (ab1801, Abcam, MA, USA) and anti-GAPDH (#2118, Cell Signaling Technology, MA, USA).

Cell viability assay (MTT assay)

MTT assay was used to evaluate cell viability after GT treatment. The assay was done by using Cell Proliferation Kit I (Roche, Netherlands). Cells (1×10^4) were seeded into a 96-well plate and incubated for 24h. Then, myoblast was treated with different concentrations of GT for 96h. After the incubation period, cells were added with 10 μl MTT solution for 4 h, then added with 100 μl solubilization solution overnight.

Absorbance was measured at 575 nm and then subtracted by background noise measured at 650 nm using a microplate reader, Multiskan GO spectrophotometer (Thermo Fisher Scientific, USA).

RNA extraction and qRT-PCR

RNA was isolated using Hybrid R (Gene All), and equal amounts of RNA were converted to cDNA using ReverTra Ace® qPCR Kit (Toyobo) according to the manufacturer's instructions. To determine gene expression levels, PCR was performed using the qPCR Master Mix Kit (Toyobo) with primer sequence shown in Table 1. Results were normalized to the level of GAPDH.

Measurement of total ROS production

C2C12 myoblast cells were incubated with TNFα (20 ng/mL) ± GT (100 ng/mL) for 4 h as indicated. Subsequently, cells were incubated with CellRox Deep Red reagent (Life Technologies, USA) for 30 min at 37°C in the darkness. Analysis was carried out on a FACS Canto or FACS Aria III (BD Biosciences, USA) at the Soonchunhyang Biomedical Research Core Facility of Korea Basic Science Institute, and data were analyzed with FlowJo software (Tree Star Inc., USA). To determine ROS levels in myotubes, differentiated C2C12 myotubes were incubated with TNFα (20 ng/mL) ± GT (100 ng/mL) for 4 h as indicated. Then, myotubes were washed, incubated with 20 μM of DCFDA solution (ab113851, Abcam) for 45 min at 37°C in the darkness, and washed with the 1X buffer according to the manufacturer's protocol. Live cells microscopy was perfomed with a filter set appropriate for fluorescein (FITC) using a fluorescence microscope (Leica). Fluorescence intensity was quantified at least ten fields of every treatment using the ImageJ software.

Hydroxyl radical scavenging assay

ROS scavenging assay was conducted as shown before [47]. Briefly, measurement of iron (II)-dependent thiobarbituric acid (TBA) reactive substance was used to assay the hydroxyl radical-mediated damage to deoxyribose. The reaction system contained 20 μl ferrous ammonium sulfate (10 mM), 50 μl of H_2O_2 (10 mM), 25 μl of EDTA (10mM), 25 μl of 2-deoxyribose, and GT in 150 μl of PBS, pH 7.4. The mixture was incubated at 37°C for 4 h. Then, 250 μl of 2.8% trichloroacetic acid (TCA) along with 250 μl of 1% TBA was added to the mixture. Then, the mixture was boiled at 100°C for 15 min, cooled and the chromogen was quantitated at 535 nm with a Multiskan GO spectrophotometer (Thermo Fisher Scientific, USA). All chemicals were purchased from Sigma-Aldrich, USA.

Mitochondrial membrane potential ($\Delta\Psi m$) assay

Mitochondrial membrane potential was examined using The MitoProbe™ DiIC1(5) Assay Kit (Molecular Probe, USA). C2C12 myoblast cells was pre-incubated with either GT (100 ng/mL) in the presence or absence of TNFα (20 ng/mL) for 24 h. Then, cells were stained with 5 μl of 10 μM DiIC1(5) for 15 min at 37°C followed by one wash in PBS buffer. Cells were pelleted by centrifugation at 1000 rpm for 5 min and resuspended in 500 μl of PBS. Fluorescence was analyzed using a FACS Canto and data were analyzed with FlowJo software (Tree Star Inc., USA). The approximate excitation and emission peaks of DiIC1(5) are 638 nm and 658 nm, respectively.

Measurement of reactive oxygen species in the mitochondria

Mitochondria superoxide production was performed using MitoSox™ Red mitochondrial superoxide indicator (Molecular Probes) according to a previous study with some modifications [47]. C2C12 myoblast cells were treated with TNFα (20 ng/mL) with/without GT (100 ng/mL) for 24 h. After that, the cells were stained with MitoSox™ (5 μM) for 10 min at 37°C and then wash in HBSS buffer one time. Cells were pelleted by centrifugation at 1000 rpm for 10 min and fixed by resuspended in 300 μl of formaldehyde (3.7%) for 10 min. The cells were pelleted by centrifugation and resuspended in 250 μl of HBSS to be analyzed by flow cytometry. Quantification was analyzed using a FACS Canto and data were analyzed with FlowJo software (Tree Star Inc., USA). The approximate excitation and emission peaks of Mitosox™ Red are 488 nm and 564-606 nm, respectively.

Gαi2 siRNA transfection

C2C12 myoblast was transfected with 5 pM of Gαi2 siRNA (Bioneer, pre-designed siRNA14678-1, 5'-GAGCAAGUUUGAGGAUCU-3', and siRNA14678-2, 5'-CCAGAGCAAGUUUGAGGA-3') and control non-targeted siRNA (Bioneer, SN-1003) using Lipofectamine RNAiMAX (Invitrogen) according to manufacturer's protocol. Differentiation was initiated after the cells were 80% confluent by changing to DMEM supplemented with 2% horse serum. The cells were differentiated for 4 days, and treated with GT (100 ng/ml) and vehicle (DMSO) for 2 days. Then, the diameter of myotubes were determined.

Animal study

C57BL/6 wild-type mice (10-weeks-old, 25 ± 1.0 g, male) were purchased from Orient (Korea). All animals were maintained in a pathogen-free environment on a 12-h light/dark cycle with free access to food and water. The handling and all experimental protocols for the mice were approved by the Soonchunhyang University Animal Care and Use Committee. The health status of all the mice used here was normal, and they were not involved in any previous experiments. To determine the anti-cancer cachexia effects of GT, LLC1 cells (2×10^6 cells) were subcutaneously injected into the right flank. When tumor was palpable at day 6, the mice were randomly divided into three groups: control health, LLC1 with PBS, and LLC1 with GEF. Mice were orally administrated daily with GEF (50 mg/kg body weight) or PBS as the vehicle control until day 21. At the end of the experiment, the tibialis anterior, gastrocnemius, EDL, and soleus muscles were harvested, and their weights were measured.

Assessment of muscle strength

Muscle performances were conducted with two independent tests. First, a grip strength test was recorded using the grip strength meter for mice (Model 47200, Ugo-Basile, Varese, Italy). To measure grip strength in the forepaws of mice, mice were gently held in the tail and allowed to grasp the metal bar. As soon as mice grasped the metal bar, the animals were pulled horizontally backwards by the tail until the grip was lost. Each mouse was evaluated in five trials at 2 min inter-trial intervals. The three maximum values of each day were normalized by dividing with body weight. The hanging test was conducted using Kondziela's inverted screen test. Each mouse was placed in the center of the wire mesh screen (40×40 cm) and then the screen was rotated slowly turned upside down and held in position 40 cm over the base. The time when mouse fell off was measured and the maximum time is 8 min. Performance was taken of three trials separated by at least 30 min.

Hematoxylin and eosin staining and immunofluorescence staining

Immunofluorescence staining of the cultured cells and cryosections was performed as described previously with slight modification [48]. Briefly, cryosections (10 μm thickness) of GA muscle were stained for 10 min in hematoxylin (Sigma-Aldrich), 3 min in eosin (Sigma-Aldrich), dehydrated with ethanol, and then cleared using Xylene solution (Daejung). Images were taken using a Nikon digital SLR camera (DS-i2) attached to the Nikon Eclipse Ti-U inverted microscope at the Soonchunhyang Biomedical Science Core Facility Center of Korea Basic Science Institute (KBSI). For immunofluorescence staining, samples were fixed with 4% formaldehyde in 1x PBS for 15 min, and then washed and blocked with 1x PBS with 5 % normal donkey serum for 1 h. Sarcomeric myosin heavy chain (MyHC) (MF20, 0.3 μg/mL; Developmental Studies Hybridoma Bank) was used. The primary antibodies were incubated overnight at 4°C. Secondary anti-mouse IgG antibody conjugated with Cy3 (1:800 dilution; Jackson Immuno-Research Laboratories, West Grove, PA, USA) was used. Cell nuclei were stained with 4′,6-diamidino-2-phenylindole (DAPI; Invitrogen, Waltham, MA, USA). The cell images were obtained using a Nikon digital SLR camera (DS-i2) attached to the Nikon eclipse Ti-U inverted microscope. The counting and measurements were carried out using ImageJ software. Evaluation of myotube diameter were determined as average diameter of at least 100 myotubes from 10 randomly chosen fields for each condition.

Statistical analysis

All *in vitro* and *in vivo* experiments were performed with three independent replicates (as indicated in the figure legends) and the results are presented as mean ± SEM (standard error mean). The sample size for each experiment is indicated in figure legends. The experimental groups were compared using a two-tailed Student's t-test and analysis of variance (ANOVA). The graphs and bar diagrams were generated using GraphPad Prism software. *P*-values < 0.05 were considered statistically significant ($^*P \leq 0.05$ and $^{***}P \leq 0.0001$).

Ethical approval and consent to participate

All protocols for this study were reviewed and approved by Institutional Review Board. The animal experiments were carried out according to Soonchunhyang University Animal Care and Use Committee.

Consent for publication

The content of this manuscript has not been previously published and is not under consideration for publication elsewhere.

CRediT authorship contribution statement

Yoseph Toni Wijaya: Visualization, Methodology, Writing – review & editing. **Tania Setiawan:** Visualization, Methodology, Writing – review & editing. **Ita Novita Sari:** Methodology, Writing - review & editing. **Seung-Yeol Nah:** Purified GT. **Hyog Young Kwon:** Project administration, Writing – original draft.

Declaration of Competing Interest

The authors declare that they have no competing interests.

Acknowledgements

This work was supported by the National Research Foundation of Korea (NRF) grant funded by the Korea government (MSIT) (No. 2020R1A2C1003791).

Supplementary materials

Supplementary data associated with this article can be found, in the online version, at 10.1016/j.neo.2021.11.008.

References

[1] Frontera WR, Ochala J. Skeletal muscle: a brief review of structure and function. *Calcif Tissue Int* 2015;**96**:183–95.

[2] Aoyagi T, Terracina KP, Raza A, Matsubara H, Takabe K. Cancer cachexia, mechanism and treatment. *World J Gastrointest Oncol* 2015;**7**:17–29.

[3] Fearon K, Arends J, Baracos V. Understanding the mechanisms and treatment options in cancer cachexia. *Nat Rev Clin Oncol* 2013;**10**:90–9.

[4] Giordano A, Calvani M, Petillo O, Carteni M, Melone MR, Peluso G. Skeletal muscle metabolism in physiology and in cancer disease. *J Cell Biochem* 2003;**90**:170–86.

[5] Baracos VE, Martin L, Korc M, Guttridge DC, Fearon KCH. Cancer-associated cachexia. *Nat Rev Dis Primers* 2018;**4**:17105.

[6] Anker MS, Holcomb R, Muscaritoli M, von Haehling S, Haverkamp W, Jatoi A, Morley JE, Strasser F, Landmesser U, Coats AJS, et al. Orphan disease status of cancer cachexia in the USA and in the European Union: a systematic review. *J Cachexia Sarcopenia Muscle* 2019;**10**:22–34.

[7] Tisdale MJ. Cachexia in cancer patients. *Nat Rev Cancer* 2002;**2**:862–71.

[8] Argilés JM, Moore-Carrasco R, Fuster G, Sl B, López-Soriano FJ. Cancer cachexia: the molecular mechanisms. *Int J Biochem Cell Biol* 2003;**35**:405–9.

[9] Marceca GP, Londhe P, Calore F. Management of cancer cachexia: attempting to develop new pharmacological agents for new effective therapeutic options. *Front Oncol* 2020;**10**.

[10] Batista ML, Peres SB, McDonald ME, Alcantara PS, Olivan M, Otoch JP, Farmer SR, Seelaender M. Adipose tissue inflammation and cancer cachexia: possible role of nuclear transcription factors. *Cytokine* 2012;**57**:9–16.

[11] Gupta SC, Kim JH, Kannappan R, Reuter S, Dougherty PM, Aggarwal BB. Role of nuclear factor kappaB-mediated inflammatory pathways in cancer-related symptoms and their regulation by nutritional agents. *Exp Biol Med (Maywood)* 2011;**236**:658–71.

[12] Zhou W, Jiang ZW, Tian J, Jiang J, Li N, Li JS. Role of NF-kappaB and cytokine in experimental cancer cachexia. *World J Gastroenterol* 2003;**9**:1567–70.

[13] Kim JH. Cardiovascular diseases and panax ginseng: a review on molecular mechanisms and medical applications. *J Ginseng Res* 2012;**36**:16–26.

[14] Zhang H, Abid S, Ahn JC, Mathiyalagan R, Kim YJ, Yang D-C, Wang Y. Characteristics of panax ginseng cultivars in Korea and China. *Molecules* 2020;**25**:2635.

[15] Sohn EH, Yang Y, Koo HJ, Park D, Kim YJ, Jang K, NamKoong S, Kang S. Effects of Korean ginseng and wild simulated cultivation ginseng for muscle strength and endurance. *Korean J Plant Resour* 2012;**25**.

[16] Cabral de Oliveira AC, Perez AC, Merino G, Prieto JG, Alvarez AI. Protective effects of Panax ginseng on muscle injury and inflammation after eccentric exercise. *Comp Biochem Physiol C Toxicol Pharmacol* 2001;**130**:369–77.

[17] Go GY, Lee SJ, Jo A, Lee J, Seo DW, Kang JS, Kim SK, Kim SN, Kim YK, Bae GU. Ginsenoside Rg1 from Panax ginseng enhances myoblast differentiation and myotube growth. *J Ginseng Res* 2017;**41**:608–14.

[18] Lee SJ, Bae J, Lee H, Lee H, Park J, Kang JS, Bae GU. Ginsenoside Rg3 upregulates myotube formation and mitochondrial function, thereby protecting myotube atrophy induced by tumor necrosis factor-alpha. *J Ethnopharmacol* 2019;**242**:112054.

[19] Go GY, Jo A, Seo DW, Kim WY, Kim Y, Ey S, Chen Q, Kang JS, Bae GU, Lee SJ. Ginsenoside Rb1 and Rb2 upregulate Akt/mTOR signaling-mediated muscular hypertrophy and myoblast differentiation. *J Ginseng Res* 2019;**44**.

[20] Hwang SH, Shin EJ, Shin TJ, Lee BH, Choi SH, Kang J, Kim HJ, Kwon SH, Jang CG, Lee JH, et al. Gintonin, a ginseng-derived lysophosphatidic acid receptor ligand, attenuates Alzheimer's disease-related neuropathies: involvement of non-amyloidogenic processing. *J Alzheimers Dis* 2012;**31**:207–23.

[21] Chei S, Song JH, Oh HJ, Lee K, Jin H, Choi SH, Nah SY, Lee BY. Gintonin-enriched fraction suppresses heat stress-induced inflammation through LPA receptor. *Molecules* 2020;**25**:1–10.

[22] Kumar RN, Ha JH, Radhakrishnan R, Dhanasekaran DN. Transactivation of platelet-derived growth factor receptor alpha by the GTPase-deficient activated mutant of Galpha12. *Mol Cell Biol* 2006;**26**:50–62.

[23] Sans-Gili MD, Lee SH, D'Alecy L, Williams J. Feeding activates protein synthesis in mouse pancreas at the translational level without changes in m-RNA. *Am J Physiol Gastrointest Liver Physiol* 2004;**287**:G667–75.

[24] Marqués M, Tranchant R, Risa-Ebrí B, Suárez-Solís ML, Fernández LC, Carrillo-de-Santa-Pau E, Del Pozo N, Martínez de Villarreal J, Meiller C, Allory Y, et al. Combined MEK and PI3K/p110β inhibition as a novel targeted therapy for malignant mesothelioma displaying sarcomatoid features. *Cancer Res* 2020;**80**:843–56.

[25] Minetti GC, Feige JN, Rosenstiel A, Bombard F, Meier V, Werner A, Bassilana F, Sailer AW, Kahle P, Lambert C, et al. Gαi2 signaling promotes skeletal muscle hypertrophy, myoblast differentiation, and muscle regeneration. *Sci Signal* 2011;**4**:ra80.

[26] Abrigo J, Elorza AA, Riedel CA, Vilos C, Simon F, Cabrera D, Estrada L, Cabello-Verrugio C. Role of oxidative stress as key regulator of muscle wasting during cachexia. *Oxid Med Cell Longev* 2018;**2018**:2063179.

[27] Nishikawa H, Goto M, Fukunishi S, Asai A, Nishiguchi S, Higuchi K. Cancer cachexia: its mechanism and clinical significance. *Int J Mol Sci* 2021;**22**:1–14.

[28] Zhu R, Liu Z, Jiao R, Zhang C, Yu Q, Han S, Duan Z. Updates on the pathogenesis of advanced lung cancer-induced cachexia. *Thorac Cancer* 2019;**10**:8–16.

[29] Cai D, Frantz JD, Tawa NE, Melendez PA, Oh BC, Lidov HG, Hasselgren PO, Frontera WR, Lee J, Glass DJ, et al. IKKbeta/NF-kappaB activation causes severe muscle wasting in mice. *Cell* 2004;**119**:285–98.

[30] Sun R, Zhang S, Lu X, Hu W, Lou N, Zhao Y, Zhou J, Zhang X, Yang H. Comparative molecular analysis of early and late cancer cachexia-induced muscle wasting in mouse models. *Oncol Rep* 2016;**36**:3291–302.

[31] Talbert EE, Metzger GA, He WA, Guttridge DC. Modeling human cancer cachexia in colon 26 tumor-bearing adult mice. *J Cachexia Sarcopenia Muscle* 2014;**5**:321–8.

[32] Cho HJ, Choi SH, Kim HJ, Lee BH, Rhim H, Kim HC, Hwang SH, Nah SY. Bioactive lipids in gintonin-enriched fraction from ginseng. *J Ginseng Res* 2019;**43**:209–17.

[33] McKinnell IW, Rudnicki MA. Molecular mechanisms of muscle atrophy. *Cell* 2004;**119**:907–10.

[34] Choi SH, Jung SW, Lee BH, Kim HJ, Hwang SH, Kim HK, Nah SY. Ginseng pharmacology: a new paradigm based on gintonin-lysophosphatidic acid receptor interactions. *Front Pharmacol* 2015;**6**:1–10.

[35] Yung YC, Stoddard NC, Chun J. LPA receptor signaling: pharmacology, physiology, and pathophysiology. *J Lipid Res* 2014;**55**:1192–214.

[36] Bonaldo P, Sandri M. Cellular and molecular mechanisms of muscle atrophy. *Dis Model Mech* 2013;**6**:25–39.

[37] Cho YJ, Choi SH, Lee RM, Cho HS, Rhim H, Kim HC, Kim BJ, Kim JH, Nah SY. Protective effects of gintonin on reactive oxygen species-induced HT22 cell damages: involvement of LPA1 receptor-BDNF-AKT signaling pathway. *Molecules* 2021;**26**:4138.

[38] Chen WM, Chiang JC, Lin YC, Lin YN, Chuang PY, Chang YC, Chen CC, Wu KY, Hsieh JC, Chen SK, et al. Lysophosphatidic acid receptor LPA3 prevents oxidative stress and cellular senescence in Hutchinson-Gilford progeria syndrome. *Aging Cell* 2020;**19**:e13064.

[39] Choi JH, Jang M, Oh S, Nah SY, Cho IH. Multi-target protective effects of gintonin in 1-Methyl-4-phenyl-1,2,3,6-tetrahydropyridine-mediated model of parkinson's disease via lysophosphatidic acid receptors. *Front Pharmacol* 2018;**9**:515.

[40] Kim HJ, Shin EJ, Lee BH, Choi SH, Jung SW, Cho IH, Hwang SH, Kim JY, Han JS, Chung C, et al. Oral Administration of gintonin attenuates cholinergic impairments by scopolamine, amyloid-β protein, and mouse model of alzheimer's disease. *Mol Cells* 2015;**38**:796–805.

[41] Park H, Kim S, Rhee J, Kim HJ, Han JS, Nah SY, Chung C. Synaptic enhancement induced by gintonin via lysophosphatidic acid receptor activation in central synapses. *J Neurophysiol* 2015;**113**:1493–500.

[42] Choi JH, Oh J, Lee MJ, Ko SG, Nah SY, Cho IH. Gintonin mitigates experimental autoimmune encephalomyelitis by stabilization of Nrf2 signaling via stimulation of lysophosphatidic acid receptors. *Brain Behav Immun* 2021;**93**:384–98.

[43] Moon J, Choi SH, Shim JY, Park HJ, Oh MJ, Kim M, Nah SY. Gintonin Administration is Safe and Potentially Beneficial in Cognitively Impaired Elderly. *Alzheimer Disease & Associated Disorders* 2018;**32**:85–7.

[44] Pyo MK, Choi SH, Shin TJ, Hwang SH, Lee BH, Kang J, Kim HJ, Lee SH, Nah SY. A simple method for the preparation of crude gintonin from ginseng root, stem, and leaf. *J Ginseng Res* 2011;**35**:209–18.

[45] Choi SH, Jung SW, Kim HS, Kim HJ, Lee BH, Kim JY, Kim JH, Hwang SH, Rhim H, Kim HC, et al. A brief method for preparation of gintonin-enriched fraction from ginseng. *J Ginseng Res* 2015;**39**:398–405.

[46] Hwang SH, Shin TJ, Choi SH, Cho HJ, Lee BH, Pyo MK, Lee JH, Kang J, Kim HJ, Park CW, et al. Gintonin, newly identified compounds from ginseng, is novel lysophosphatidic acids-protein complexes and activates G protein-coupled lysophosphatidic acid receptors with high affinity. *Mol Cells* 2012;**33**:151–62.

[47] Sari IN, Yang YG, Wijaya YT, Jun N, Lee S, Kim KS, Bajaj J, Oehler VG, Kim SH, Choi SY, et al. AMD1 is required for the maintenance of leukemic stem cells and promotes chronic myeloid leukemic growth. *Oncogene* 2021;**40**:603–17.

[48] Sah JP, Hao NTT, Han X, Tran TTT, McCarthy S, Oh Y, Yoon JK. Ectonucleotide pyrophosphatase 2 (ENPP2) plays a crucial role in myogenic differentiation through the regulation by WNT/β-Catenin signaling. *Int J Biochem Cell Biol* 2020;**118**:105661.